ACS SENSORS

pubs.acs.org/acssensors
Article

Identification of Gas Mixture Components with Multichannel Hierarchical Analysis of Time-Resolved Hyperspectral Data

Eunji Choi,[#] Tae-In Jeong,[#] Thanh Mien Nguyen,[#] Alexander Gliserin, Jimin Lee, Gyeong-Ha Bak, San Kim, Sehyeon Kim, Jin-Woo Oh,* and Seungchul Kim*

Cite This: ACS Sens. 2025, 10, 3003−3012

Read Online

ACCESS | Metrics & More | Article Recommendations | Supporting Information

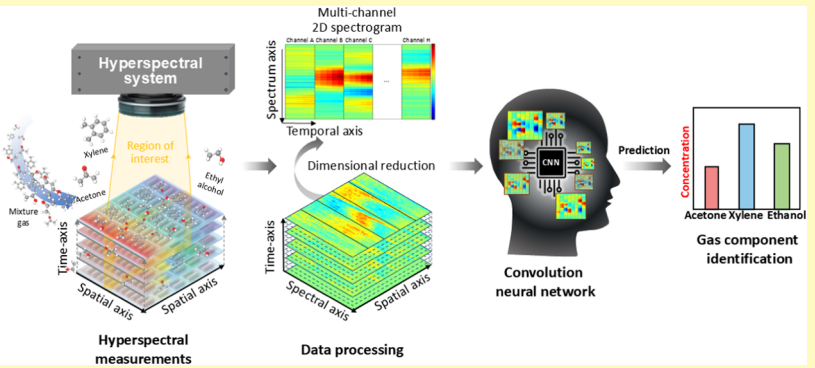

ABSTRACT: Chemical vapor sensors are essential for various fields, including medical diagnostics and environmental monitoring. Notably, the identification of components in unknown gas mixtures has great potential for noninvasive diagnosis of diseases such as lung cancer. However, current gas identification techniques, despite the development of electronic nose-based sensor platforms, still lack sufficient classification accuracy for mixed gases. In our previous study, we introduced multichannel hierarchical analysis using a time-resolved hyperspectral system to address the spectral ambiguity of conventional RGB sensor-based colorimetric e-noses. Here, we demonstrate the identification of mixed gas components through time-resolved line hyperspectral measurements with an eight-colorimetric sensor array that uses genetically engineered M13 bacteriophages as gas-selective colorimetric sensors. The time-dependent spectral variations induced by mixed gas in the different colorimetric sensors are converted into a hyperspectral three-dimensional (3D) data cube. For efficient machine learning classification, the data cube was converted into a multichannel spectrogram by applying a novel data processing method, including dimensionality reduction and a block average filter to reduce high-dimensional complexity and improve the signal-to-noise ratio. A convolution filter was then used for hierarchical analysis of the multichannel spectrogram, effectively capturing the complex gas-induced spectral patterns and temporal dynamics. Our study demonstrates a classification accuracy of 93.9% for pure and mixed gases of acetone, ethanol, and xylene at a low concentration of 2 ppm.

KEYWORDS: *gas mixture component identification, hyperspectral analysis, hierarchical analysis, colorimetric sensor, electronic nose*

Chemical vapor sensors play a crucial role in numerous scientific and industrial applications, most notably in medical diagnosis and environmental monitoring.[1−4] Recently, the importance of complex gas component identification has been demonstrated for disease diagnosis. In particular, several studies have demonstrated that the identification of target volatile organic compounds (VOCs) from human exhaled gas enables disease diagnosis, including lung cancer.[5−8]

Electronic nose (e-nose) technologies mimic the human olfactory system to detect and identify target gases and VOCs by using an array of chemical sensors, each sensitive to specific types of molecules.[9−11] When exposed to a gas, an array of sensors generates a fingerprint based on the species of the gas or a component within a gas mixture. This pattern is recognized and trained with machine learning (ML) to identify and classify VOCs with a high accuracy of the classification. To date, various signal processing and ML algorithms, such as the k-nearest neighbors (KNN) algorithm,[12,13] support vector machine (SVM),[14−16] or principal component analysis (PCA),[17−19] have been extensively studied for gas classification. In particular, convolutional neural networks (CNN) have demonstrated outstanding abilities to capture spatial patterns

Received: January 2, 2025
Revised: March 11, 2025
Accepted: March 18, 2025
Published: March 24, 2025

https://doi.org/10.1021/acssensors.5c00015
ACS Sens. 2025, 10, 3003−3012

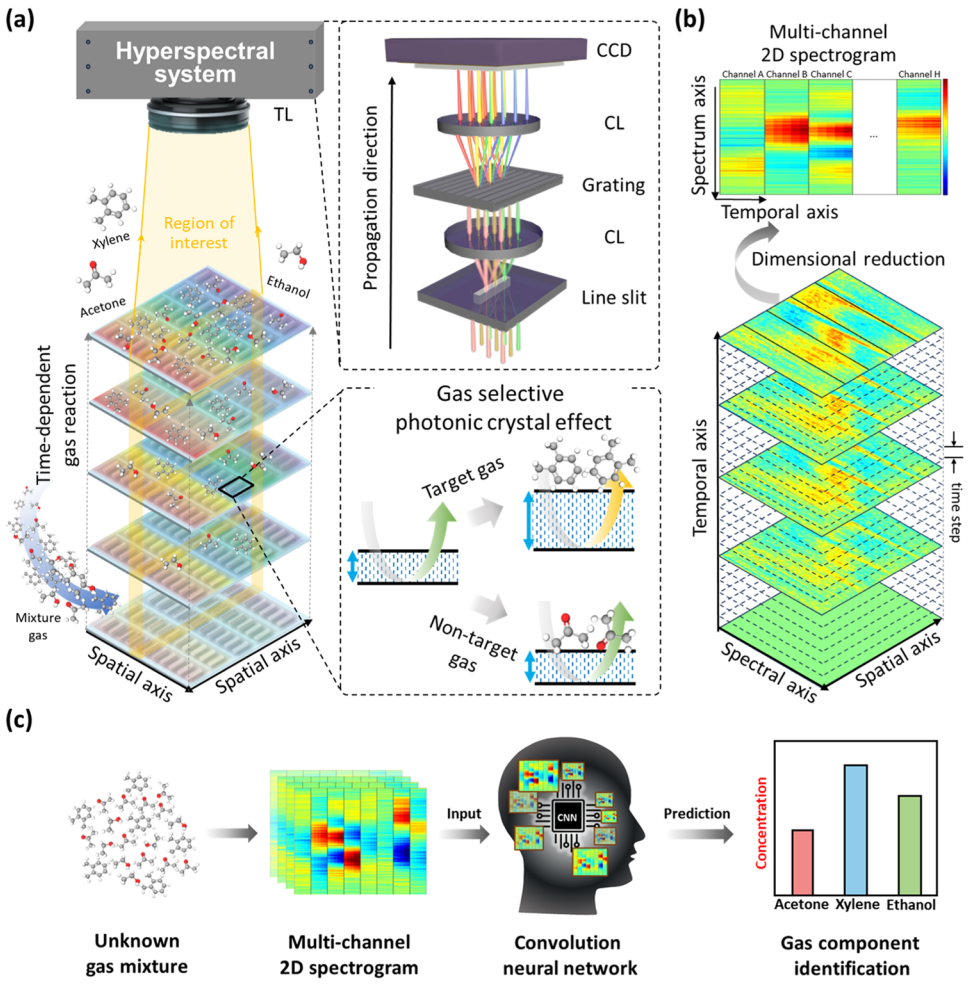

Figure 1. Principle of the time-resolved hyperspectral measurement for complex gas classification. (a) Schematic of the time-resolved hyperspectral measurement process with a colorimetric 1D line array sensor stimulated by complex gas molecules. The diffraction angle of the illuminated white light (WL) on each colorimetric sensor is changed due to the gas-selective photonic crystal effects of the phage bundles stimulated by the target gases. The 1D line hyperspectral system records a spectrum for every point on the line slit perpendicular to the slit on the imaging detector. CL, collimating lens; CCD, charge-coupled device. (b) Measured time-resolved hyperspectral data is dimensionally reduced and rearranged into a multichannel 2D spectrogram. (c) Schematic of the gas component identification process using a multichannel spectrogram-based CNN model.

and hierarchical features in visual data.[20−22] The utilization of a convolution filter enables the model to learn while maintaining the association between neighboring pixels, thereby conserving spatial information and features.

Chemoresistive gas sensors have demonstrated high sensitivity for detecting a target gas based on the interaction between the material and the target gas;[23−26] however, the inherent limitation on expansion of reactive gas species in chemoresistive type makes them not suitable for multigas classification.[27,28] In contrast, colorimetric sensors are promising for e-nose-based complex gas component detection due to their relatively simple sensor array manufacturing method and gas selectivity of each sensor[29−32] and have already demonstrated excellent performance for multigas component identification.[33−35] However, multigas identification in complex gas mixtures is still challenging and requires advanced measurement and data processing methods. Conventional colorimetric e-nose sensor systems utilize RGB optical detectors to measure colorimetric changes in the sensor with only three (red, green, blue) wide-band spectral channels, which cannot capture the complete spectral response of the colorimetric sensor array and therefore lose much information about its spectral variation.[36] In our previous study, which focused on introducing a new system, we developed a new hierarchical analysis of a multichannel spectrogram with a line hyperspectral sensor system and verified its superior performance by comparison with a conventional RGB detector.

In this study, we demonstrate the identification of multigas components in a gas mixture via multichannel hierarchical analysis of time-resolved hyperspectral (TRH) data, utilizing the line hyperspectral measurement-based multichannel spectrogram. Unlike our previous study, which introduced advanced hierarchical analysis using three-dimensional (3D) hyperspectral data, we exploited this technique for the first time for the identification of a gas mixture at a low concentration level. Acetone, ethanol, and xylene were used as target gases because these gases are not only common in our living environment but also harmful to the human body, and furthermore, detecting these gases in a gas mixture and analyzing their components have the potential for noninvasive lung cancer diagnosis.[5,37,38] Our results showed a 93.9% classification accuracy of both pure and gas mixture components at a low concentration level of 2 ppm. The increased classification performance was achieved by applying

https://doi.org/10.1021/acssensors.5c00015
ACS Sens. 2025, 10, 3003−3012

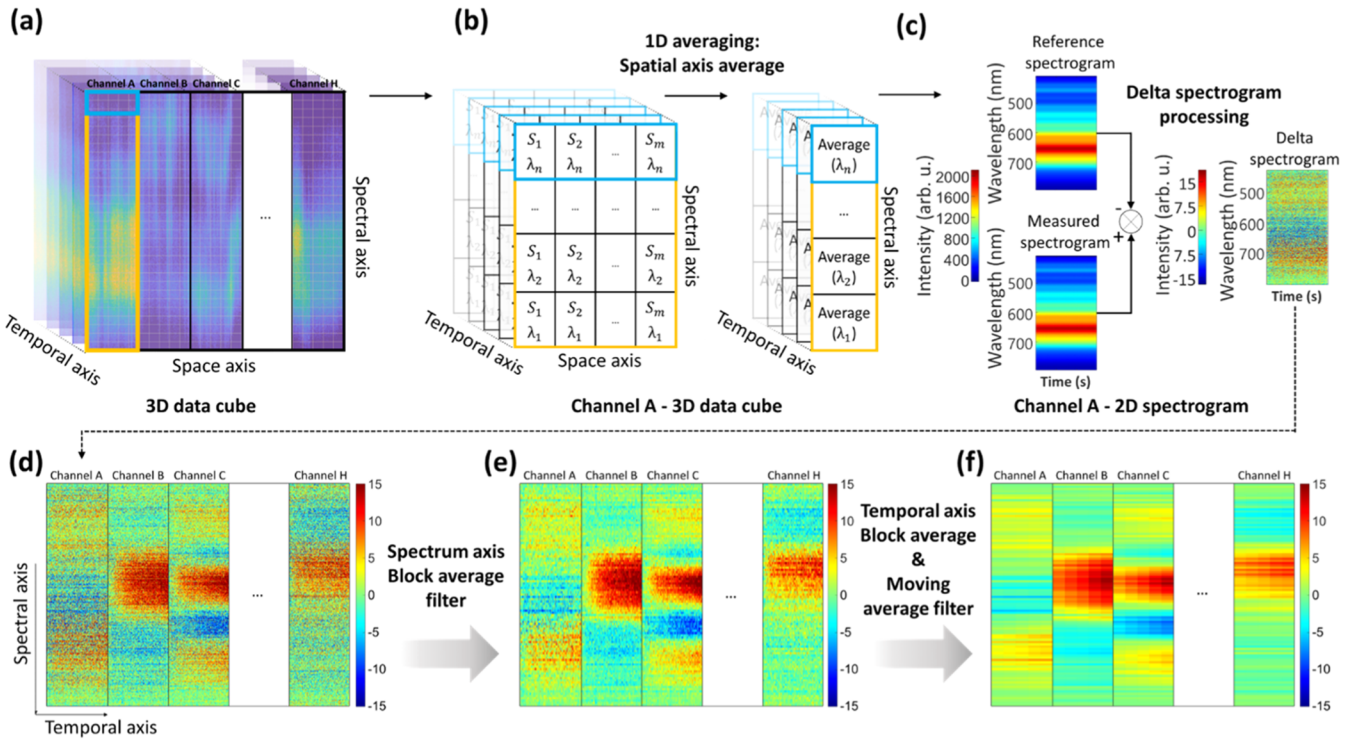

Figure 2. Data processing and filtering sequence of the multichannel spectrogram. (a) Schematic illustration of the 3D data cube, spatially segmented into discrete channels with different sensor properties. (b) Dimensionality reduction from 3D to 2D is achieved by averaging the time-resolved spectra across all spatial pixels within each channel. (c) Computing a delta spectrogram by subtracting the reference spectrum from the measured spectrogram. (d) Multichannel delta spectrogram without filtering. (e) Data processed using a block average filter applied along the spectral axis. (f) Data filtered with a multifilter, which applies both a block average and a moving average filter along the temporal axis; data processing and filtering are performed independently for each channel.

selective spectral and temporal filters to the multichannel spectrograms in a low-gas concentration environment. The multichannel spectrograms were trained with a CNN for hierarchical analysis, enabling feature recognition of spectral patterns and temporal dynamics in the spectrograms, which allowed robust classification of gas components within gas mixtures. This demonstrated advanced gas mixture identification performance has great potential for noninvasive disease diagnostics, including lung cancer detection, due to the inherent complexity of human breath composition and the subtle biochemical variations induced by disease.

RESULTS AND DISCUSSION

Principle of the Time-Resolved Hyperspectral Measurement for Complex Gas Classification. The TRH system records the time dependence of a spectral change in a colorimetric sensor line array during its interaction with a complex gas (Figure 1a). The line hyperspectral measurement is performed by a custom-built line-scan imaging device. It consists of a dispersive spectrograph (SPECIM, ImSpector V10E) with a telecentric lens (SPO, TCL0.8X-160−4M) to achieve a planar image plane and minimize angular aberrations and is coupled to an electron-multiplying CCD (EMCCD) image sensor (Andor, Luca DL-640M) with a resolution of 1004 × 1002 pixels. The visible wavelength ranges from 400 to 800 nm and spans approximately 517 pixels on the image sensor, and a subset of this range between 410 and 795 nm was used in this work, covering 496 pixels. A radiometrically calibrated incandescent tungsten halogen lamp (OceanOptics, HL-3P-CAL) was used for intensity calibration of the raw spectra from the image sensor prior to the measurements. This setup enables automated time-resolved spectroscopy of a fixed line region or a full-image hyperspectral scan of an object by scanning the sample stage. In this work, TRH data was acquired as a line section at a fixed sample position, providing a time-varying spectrum for each image pixel along the line. The achievable time resolution in this mode is limited by the minimum image acquisition time of the EMCCD sensor, approximately 33 ms, which is sufficient to capture the spectral response dynamics of the bacteriophage sensors studied in this work. Here, a 500 ms time interval was used for data acquisition of over 600 s. The sampling rate of 500 ms was selected by the consideration of the response time of the employed M13 bacteriophage-based colorimetric sensor. The response time of the genetically engineered M13 bacteriophage was investigated as a VOC stimulation. Real-time light scattering measurements were conducted every 50 ms under ethanol stimulation by using a commercial spectrometer. Upon exposure to ethanol, a red shift in the scattered light was observed with a rapid response time of approximately 850 ms, as depicted in Figure S1a. Moreover, a response time of 500 ms was observed for H_2O molecules, which exhibit a relatively higher binding affinity and fast response time compared to other VOCs.[36,39] Thus, a sampling rate of 500 ms can provide the hyperspectral data that captures the dynamic response behavior of the M13 bacteriophage sensor. The colorimetric sensor array was arranged along this line, with each channel predefined as a contiguous segment of line pixels assigned along the line section to divide the data with each colorimetric sensor. The scattered light from the colorimetric sensor array is

https://doi.org/10.1021/acssensors.5c00015
ACS Sens. 2025, 10, 3003−3012

collinearly collected with a telecentric lens and enters the one-dimensional (1D) line slit of the hyperspectral system. Here, an optical grating projects the spectrum of each point along the line slit orthogonally to the slit onto a CCD camera, thus transforming the 1D line slit image into a 2D hyperspectral image consisting of one spatial axis and one spectral axis.

We employed the M13 bacteriophage as the gas-selective component of the colorimetric sensor, which exhibits a dynamic photonic crystal effect upon gas stimulation,[40] and genetic engineering allows assigning unique gas selectivity for each colorimetric sensor (see the Supporting Information for details). This photonic crystal effect is facilitated by the self-alignment of the M13 bacteriophages into bundles with a high surface-to-volume ratio through the pulling method (Figure 1a). We employed a standardized fabrication process with precise control over the pulling speed, ensuring the stable reproducibility of the sensor.[41] The repeatability of the utilized colorimetric sensor is demonstrated in Figure S1b through repeated ethanol exposure experiments, confirming consistent performance across multiple cycles. In addition, the chromaticity plot of the color change is shown in Figure S1c in CIE coordinates, depicting distinct color changes with a red shift of the initial green under ethanol stimulation. Additionally, the long-term stability test was conducted over two months using TRH measurements, confirming that the sensors maintained consistent performance without significant degradation, thereby supporting their sensing reliability (Figure S2). The photonic crystal effect of the M13 bacteriophage upon gas stimulation arises from intermolecular interactions between its capsid proteins and target molecules. Since these interactions are weaker than intramolecular forces, the chemical structure of the capsid proteins remains intact even after repeated use, ensuring long-term stability.

The measured TRH data are initially accumulated into a 3D data cube, which consists of one spatial, one spectral, and one time dimension (Figure 1b). This high dimensionality of the 3D data cube increases the complexity of data processing and deep learning (DL) training;[42,43] therefore, the 3D data cube is dimensionally reduced into a 2D multichannel spectrogram (see details below), which enables us to solve the high-dimensional complexity but also substantially simplifies and accelerates the hierarchical analysis with the CNN model. Processing a multichannel spectrogram with a CNN captures not only the spectral and temporal changes of each sensor but also the hierarchical relations, including reactivity and response time relationships within the sensor array. The identification of pure and gas mixture species was conducted using an e-nose-based artificial intelligence architecture, specifically a multichannel spectrogram-based CNN model (Figure 1c), which classifies the chemical vapor composition based on the multichannel spectrogram features via a convolution filter and hierarchical analysis after successful training.

Hyperspectral Data Processing: Dimensionality Reduction and Feature Extraction. The hyperspectral data obtained during the gas reaction at the colorimetric sensor form a 3D data cube with three axes—spatial, spectral, and temporal—and contain time-resolved spectral information from the sensor array (Figure 2a). The abundant information on colorimetric sensors within the 3D data cube leads to high-dimensional complexity and a large data volume. This not only entails substantial computational challenges for ML models but also limits the noise robustness of the colorimetric sensor in a low gas concentration environment, since the signal is distributed over a large data volume, leading to reduced signal-to-noise ratio (SNR). The high-dimensional complexity and noise limitations can be alleviated through our data processing method for dimensional reduction. First, the 3D data cube is decomposed into individual spatial regions, or channels, corresponding to each genetically engineered phage sensor. Due to the linear configuration of the 1D spatial axis in our line hyperspectral system, the colorimetric sensor array is recorded simultaneously, enabling the extraction of spatially separated signals from each channel. Since the phage types are identical within such a region, the spectral properties do not vary along the spatial axis within a channel, except due to noise and nonuniformities of the sensors (Figure 2a). Second, each channel's 3D data cube is reduced to two dimensions by averaging along the spatial axis during the measurement, which results in a 2D spectrogram with a time and wavelength axis (Figure 2b). Since bacteriophages of the same genotype exhibit uniform color change responses due to their identical physicochemical properties, spatial averaging is confined to sensors with the same molecular composition. Although minor signal variations may arise from surface roughness during the self-assembly of M13 bacteriophages, this targeted averaging reduces localized noise, enhances the signal-to-noise ratio (SNR), and ensures a stable spectral response. Additionally, reducing the data complexity through spatial averaging enables more efficient data processing. Third, a delta spectrogram is obtained by subtracting the reference spectrogram, which is composed of the reference spectrum measured without the gas from the spectrogram acquired during the gas exposure (Figure 2c). The delta spectrogram processing extracts only the time-dependent spectral variations induced by the gas stimulation in the colorimetric sensor to amplify dynamic changes, which also improves the SNR. However, the generated delta spectrogram still contains significant noise in a low-gas concentration environment with systematic noise from the light source and detector (Figure 2d). Fourth, a filtering process is applied for noise reduction, employing a block average filter along the spectral axis, which averages every set of five spectra (Figure 2e). This averaging process improves the SNR by reducing the density of spectral samples in the hyperspectral data, which contains a significant amount of redundant information,[44] including a high degree of correlation between many spectral bands. Lastly, a multifilter is applied along the temporal axis consisting of a sequential block average filter binning the temporal axis into five time segments and a moving average filter (Figure 2f). Each channel is independently processed in this way, and the resulting 2D spectrograms from each channel are concatenated along the temporal axis to obtain a multichannel 2D spectrogram (Figure S3). Therefore, the multichannel 2D spectrogram contains a periodic temporal axis, which sequentially represents the bacteriophage sensor regions with different chemical properties.

Multichannel Spectrogram Analysis with Genetically Engineered Bacteriophage-Based Colorimetric Sensor Arrays. The M13 bacteriophages were genetically engineered to assign gas selectivity through surface modifications of the capsid protein (pVIII) for tailored chemical functionalities. These modifications exploit the genetic versatility of M13 bacteriophages, enabling us to incorporate amino acids with specific chemical properties that influence their interactions with VOCs. Here, we have developed a highly integrated color sensor array consisting of eight genetically engineered M13 bacteriophages (Figure 3a). The number of measurable sensors

https://doi.org/10.1021/acssensors.5c00015
ACS Sens. 2025, 10, 3003−3012

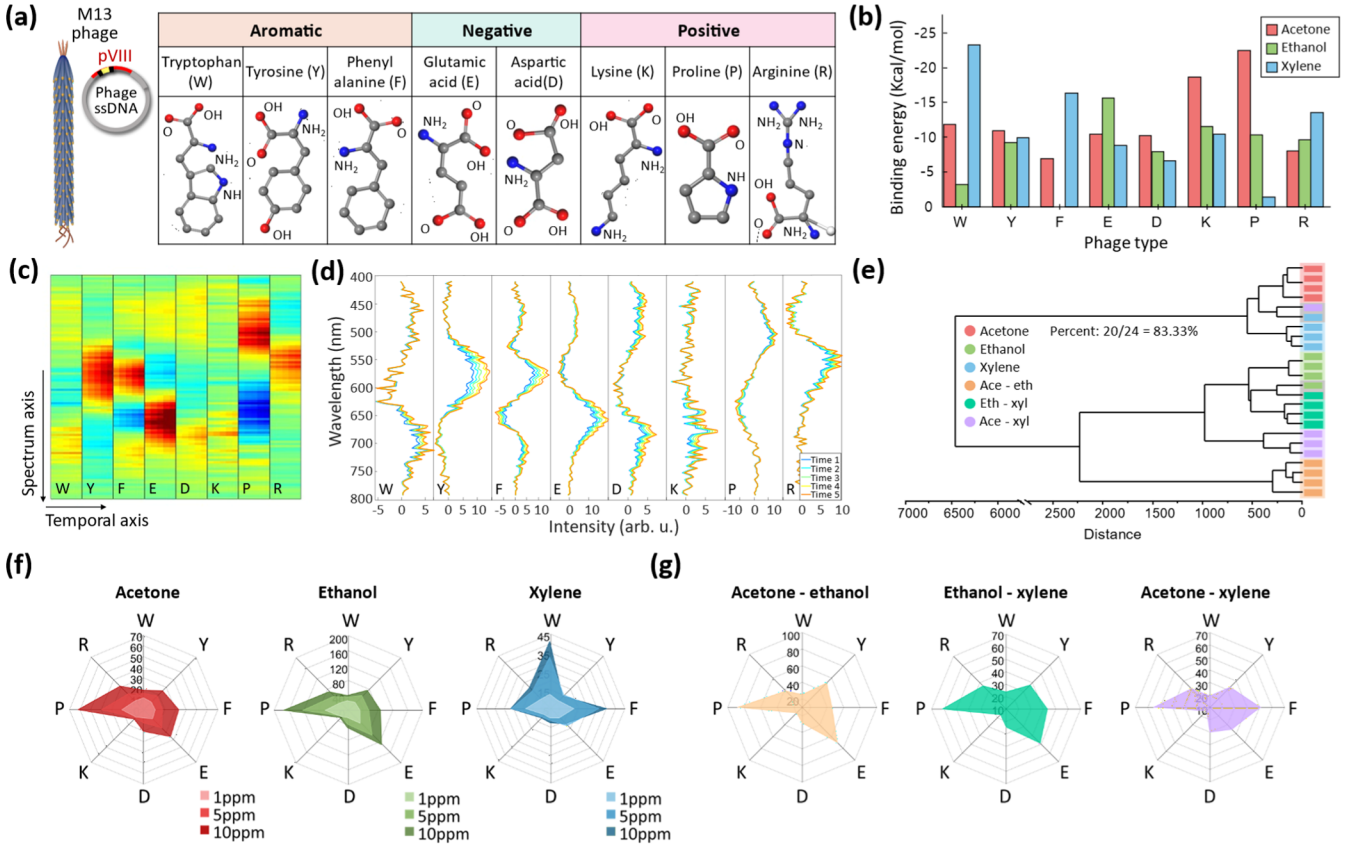

Figure 3. Multichannel spectrogram analysis with genetically engineered bacteriophage-based colorimetric sensor arrays. (a) Chemical structure of amino acids representing the functional capsid proteins and schematic illustration of a genetically engineered bacteriophage. (b) DFT-based binding energy calculations between various amino acids and acetone, ethanol, and xylene gas, respectively. (c) Multichannel spectrogram results for gas stimulation with ethanol (2 ppm concentration). (d) Spectral intensity variation of the multichannel spectrogram (c) in five different time regions. (e) Hierarchical clustering analysis (HCA) for VOC classification based on color distance. (f, g) Color distance fingerprint from eight different types of phage sensor arrays for various single gas (f) concentrations (1, 5, 10 ppm) and gas mixtures (g) with 2 ppm concentration.

can be adjusted by employing a telecentric lens with an optimal numerical aperture. By manipulating the gene encoding the pVIII protein, we integrated amino acids from a natural library of 20 common amino acids. These included residues with distinct electrical charges (positively charged lysine [K], arginine [R], and proline [P]; negatively charged glutamic acid [E], and aspartic acid [D]), as well as hydrophobic side chains (tryptophan [W], tyrosine [Y], and phenylalanine [F]) (Figure 3a, right table). This resulted in phages with chemically diverse surfaces, grouped into three categories based on their dominant interaction modes: (1) negative charge interactions involving residues like lysine (K), arginine (R), and glutamic acid (E); (2) positive charge interactions facilitated by residues like aspartic acid (D) and proline (P), and (3) $\pi-\pi$ stacking interactions involving aromatic residues like tryptophan (W), tyrosine (Y) and phenylalanine (F). This customization enables the sensor to selectively interact with VOC molecules based on their chemical properties, such as polarity, charge, and aromaticity. To validate the observed selectivity, density functional theory (DFT) simulations were performed to calculate the binding energies of each amino acid residue with the corresponding VOC molecules, as shown in Figure 3b (detailed geometry optimization is shown in Figure S4). These simulations modeled molecular interactions at the atomic level and guided the selection of surface modifications, leading to the identification of configurations that enhance sensor performance, improving both sensitivity and selectivity for detecting specific VOCs. While this study focuses on acetone, ethanol, and xylene, which are related to noninvasive lung cancer diagnosis, the M13 bacteriophage sensor is not restricted to these gases.[41,45] The time-resolved colorimetric response in each genetically engineered phage sensor was recorded with the hyperspectral system and processed into a multichannel spectrogram; Figure 3c shows the multichannel spectrogram with 2 ppm concentration of ethanol gas stimulation. The interconnected regions sequentially show the distinct colorimetric dynamics of each genetically engineered phage sensor, including the spectral range, speed, and intensity of the reaction. The multichannel spectrogram was disassembled to observe the spectral response for phage species in five different time regions representing consecutive intervals after the initial gas exposure (Figure 3d). Each sensor exhibits spectral variations in different wavelength ranges, and especially the spectral response of phage sensor F case is tricky to record with a conventional RGB detector because of the cancel out effect from the broad response bandwidth of each RGB detector.[36] Additionally, the spectral response in the colorimetric sensor array when exposed to pure and gas mixtures was recorded with the hyperspectral system, which exhibits distinct spectral intensity variations and response rates depending on the gas type (Figure S5).

Color distance (CD) is a commonly used metric for quantitative analysis of measured color changes. The time-dependent CD of the 2D multichannel spectrogram was

https://doi.org/10.1021/acssensors.5c00015
ACS Sens. 2025, 10, 3003−3012

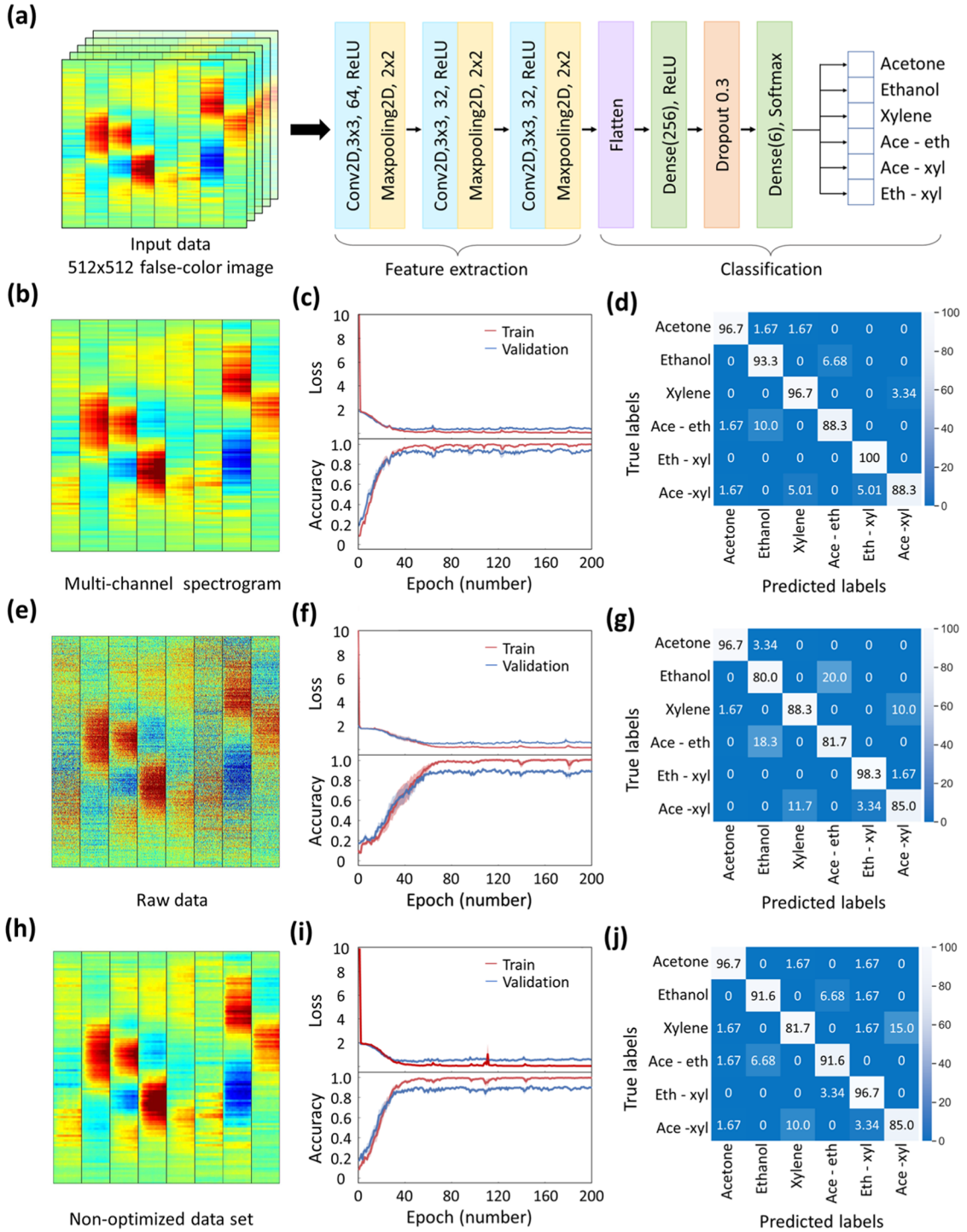

Figure 4. Hierarchical analysis of multichannel spectrograms via CNN. (a) Architecture of the proposed CNN for classifying the six gas types (i.e., acetone, ethanol, xylene, acetone/ethanol, ethanol/xylene, and acetone/xylene). (b) Multichannel spectrogram with optimized data processing. (c, d) Loss, accuracy (c), and confusion matrix (d) result for CNN model trained with multichannel spectrogram. (e) Multichannel spectrogram without data processing. (f, g) Loss, accuracy (f), and confusion matrix (g) result for CNN model trained with nondata processed multichannel spectrogram. (h) Multichannel spectrogram with nonoptimized data processing. (i, j) Loss, accuracy (i), and confusion matrix (j) result for CNN model trained with nonoptimized data processed multichannel spectrogram.

calculated by summing the absolute spectral intensity changes at each wavelength by comparing the measured spectral intensity and the initial spectral intensity (Figure S6). The dynamic CD response of the system with various target gases (acetone, ethanol, and xylene) at different concentrations (1, 2, 5, and 10 ppm) represents the system's capability to analyze gases across different concentration levels (Figure S7) and gas mixtures (Figure S8). The time-dependent CD of the genetically engineered phage-based color sensors increases upon gas exposure, with a varying rate of increase depending on the gas type. This provides a dynamic view of the reactivity of the sensor toward VOCs, with each bacteriophage type

https://doi.org/10.1021/acssensors.5c00015
ACS Sens. 2025, 10, 3003−3012

displaying a unique response signature based on its surface chemistry, as studied in DFT simulations. These time-response curves show an asymptotic behavior, reaching saturation after prolonged exposure to the target gas.

Hierarchical clustering analysis (HCA) and PCA were performed by using the time-dependent CD (Figure S9). The HCA classification accuracy for pure and gas mixtures at 2 ppm concentration is 83.33%, which reveals a relatively low classification accuracy (Figure 3e). This result shows that conventional time-dependent CD value analysis is insufficient for classifying low-concentration level gas mixture components and necessitates the multichannel spectrogram-based DL analysis method. Nonetheless, the CD fingerprint from eight different types of phage sensor arrays shows their unique signature patterns upon reacting with various gases (acetone, ethanol, and xylene) and concentrations (1, 5, and 10 ppm), indicating that our system not only has linear concentration-dependent reactivity but also selectivity for different VOCs (Figure 3f). The CD value of the CD fingerprint was calculated by averaging time-dependent CD (Figure S6). The bacteriophages containing proline (P) and glutamic acid (E) showed strong reactivity toward acetone and ethanol but a relatively lower response to xylene. Conversely, phages with hydrophobic amino acids, such as tryptophan (W) and tyrosine (Y), exhibited strong responses to xylene, attributed to the $\pi-\pi$ stacking interactions with the aromatic rings of xylene molecules. This experimental result, correlated with the DFT result, indicates that residues with aromatic side chains have higher binding affinities for aromatic VOCs like xylene, while charged and polar residues show stronger interactions with polar solvents like acetone and ethanol. Additionally, the CD fingerprint patterns of 1:1 ratio gas mixtures (2 ppm concentration of each gas) show subtle differences depending on the stimulated gas (Figure 3g). The engineered bacteriophage types demonstrate high selectivity, even when measured in complex gas mixtures. P-type and E-type strongly interact with the mixtures containing acetone and ethanol, while the F-type shows a strong response with xylene gas, as demonstrated with single gases.

Hierarchical Analysis of Multichannel Spectrograms via Convolutional Neural Networks. The multichannel 2D spectrogram generated from the 3D data cube measured by hyperspectral imaging exhibits a complexity that makes it challenging to analyze such colorimetric measurements using simple algorithms. DL approaches are highly effective in extracting features from complex data. In particular, CNN excels at capturing spatial patterns and hierarchical features through its layered architecture, automatically extracting deep features, which has been proven to be highly successful in visual tasks such as image classification.[22] The CNN framework is particularly effective for analyzing the multichannel 2D spectrogram data for several reasons. First, the 2D convolutional filters in the CNN architecture share weights across both spectral and temporal dimensions, allowing for efficient extraction of spatial features enriched with spectral information from the multichannel 2D spectrogram. Additionally, it can learn while maintaining the relationships between adjacent data points across both the wavelength and temporal dimensions, capturing the gradual spectral shifts that occur during the interactions of the colorimetric material with the gas.[46,47] Second, pattern recognition in multichannel spectrograms, which are composed of spectrograms from spatially distinct channels, allows capturing of both the spectral characteristics of each channel and the hierarchical relationships between channels.[36] Consequently, analyzing multichannel 2D spectrograms using CNN provides a comprehensive understanding of both local features and hierarchical relationships, making it highly effective for recognizing complex patterns in the temporal and spectral data of colorimetric sensors with multiple channels as well as the relationships between channels.

The CNN architecture used for selective gas detection is applied to the preprocessed multichannel 2D spectrogram data collected from our gas sensor array targeting six different gas compositions (Figure S10). The architecture of the CNN model consists of three convolutional layers, followed by a flattening layer. Each convolutional layer applies a 2D convolution with a kernel size of 3×3, using the ReLU as the activation function, followed by a max-pooling layer with a pool size of 2×2 to effectively extract features. The final dense layer, with 6 units and a softmax activation function, is used for classification (Figure 4a).[48] The CNN model utilizes multiple convolutional layers to simultaneously reduce the dimensionality of the input data and extract important features, thus preventing information loss while unavoidable sensor background drift and system noise are removed, thereby enhancing classification accuracy.

The loss and accuracy curves (Figure 4c) represent the learning process of the model, showing the training (red) and validation (blue) parts. There is no significant difference between the training and validation sets, indicating that the model did not suffer from overfitting and that the data were well classified throughout the training iterations. The confusion matrix shows the distribution of the model's predictions across the true labels, with each cell representing the percentage of instances that were classified into a specific category. The percentages along the principal diagonal reflect the model's accuracy in correctly classifying the data. The accuracy was calculated by dividing the number of correctly classified samples by the total number of samples in the validation data set. The accuracy values and other metrics presented were averaged over ten repeated runs across five different data sets, providing a comprehensive view of the model's performance across various scenarios. Each data set was utilized with randomly selected samples for training and validation, demonstrating the robustness of the CNN model in classifying the multichannel 2D spectrogram data set. The CNN model achieved an average accuracy of 93.9% with a standard deviation of 3.24% for the gas composition classification and achieved a maximum accuracy of 97.22% (Figure 4d and Table S1). The Grad-CAM method was utilized to enhance the transparency of the CNN model's classification decision process and improve its interpretability. The Grad-CAM visualizes the spectral and temporal regions that are most influential in the classification decisions of the 2D multichannel spectrogram-based CNN model (Figure S11). The results highlight specific spectral regions and temporal features that significantly contribute to gas composition identification, demonstrating that the model effectively captures key spectral patterns relevant to classification. Furthermore, to evaluate the model's generalization ability and ensure that it does not overfit to any specific data set, we additionally performed k-fold cross-validation, which resulted in an average accuracy of 92.22%, demonstrating that the model performs consistently well across different data partitions (Figure S12).

https://doi.org/10.1021/acssensors.5c00015
ACS Sens. 2025, 10, 3003−3012

Table 1. Summary of Machine Learning-Based Gas Mixture Identification Research in the Last Three Years[a]

sensor type	number of test gases	target gases	concentration of gases	analysis method	classification accuracy (%)	refs
phages	3	acetone, ethanol, xylene	2 ppm	CNN	93.9	this work*
QCM + nanoporous MOF films	3	p-, o-, m-xylene	10 ppm, 100 ppm	kNN	96.5	13
SERS	4	acetophenone, anisole, anethole, benzaldehyde		SVM	99.4	14
SMO + micro-LED	2	ethanol, methanol	0−100 ppm	D-CNN	97.0	49
MDFG	4	NO_2, NO, NH_3, H_2S	10 ppm	SVM, 1D CNN	100	50
MOS	2	NO_2, CO	0−50 ppm	CNN	100	51
YSZ-based mixed potential sensor	3	isoprene, *n*-propanol, acetone	10−30 ppm	KNN/SVM	99	52

[a]SMO semiconductor metal oxides; MDFG multiplexed DNA-functionalized graphene; QCM quartz crystal microbalance; MOF metal−organic frameworks; MOS metal−oxide−semiconductor; SERS surface-enhanced Raman scattering; YSZ yttria-stabilized zirconia; D-CNN deep convolutional neural network; SVM support vector machine; and KNN k-nearest neighbor algorithm.

To demonstrate the superiority of the utilized CNN algorithm, we applied the 2D multichannel spectrogram data to PCA and SVM algorithms. The PCA and SVM achieved classification accuracies of 81.95 and 87.78%, respectively, both of which were lower than the CNN's 93.9% accuracy (Table S2). This performance gap arises because both PCA and SVM struggle to capture nonlinear patterns and hierarchical relationships within the data. In contrast, the convolutional filters in the CNN model enable the efficient extraction of hierarchical and nonlinear features, resulting in superior classification accuracy compared to other deep learning algorithms. In addition, we performed a batch-to-batch dependence analysis with six distinct batch groups to assess the impact of batch-to-batch variability on the classification performance (Figure S13). Groups 1 and 3 consist of genetically engineered bacteriophages with similar chemical properties, whereas Groups 2 and 4 represent modified versions of these groups with additional chemical characteristics. Groups 5 and 6 consist of bacteriophages with distinct chemical properties (Figure S13a). The heatmap of classification accuracy demonstrates that batches containing sensors with similar chemical properties exhibit lower classification accuracy than those with more chemically diverse properties despite an equivalent number of sensors (Figure S13b). The multiarray sensor, composed of genetically engineered bacteriophages with diverse chemical properties, significantly improves VOC differentiation and overall classification performance. This emphasizes the successful configuration of the bacteriophage batches, which were designed using bacteriophage strains with high reactivity to target gases.

The necessity of the optimized data processing method was demonstrated by training the CNN model with the raw data set and nonoptimized data processing data set. Note that the nonoptimized data process refers to a smaller window size of moving averaging filter data process than the optimized data process. The CNN model trained with the raw data set shows a classification accuracy of 88.06% (Figure 4e−g and Table S1). Furthermore, the CNN model trained with a nonoptimized data processing data set shows a classification accuracy of 90.28%, which demonstrates our optimized data processing method results in a higher classification accuracy by increasing the SNR (Figure 4h−j and Table S1). Additionally, the performance of the classifier was evaluated by plotting the receiver operating characteristic (ROC) curve, which compares the true positive rate and false positive rate. The ROC curve shows that our model achieved high accuracy with an average area under the curve (AUC) score of 0.967 (Figure S14), indicating that the CNN model reliably distinguishes between the six different gas compositions. The model's performance, as demonstrated through various evaluation metrics, highlights its suitability for accurate and reliable gas component detection.

CONCLUSIONS

In this study, we demonstrated the successful classification of gas components in pure and gas mixture at 2 ppm concentration via a hierarchical analysis of the multichannel spectrogram obtained by TRH imaging of a genetically engineered M13 bacteriophage colorimetric sensor array. In Table 1, this study is compared with recent ML-based gas mixture identification research. While most previous studies utilized relatively high gas concentrations for the gas mixtures component identification, our study classified pure and mixed gas components at only 2 ppm concentration. The advanced performance of our system was made possible by (1) application-specific data processing of the hyperspectral 3D data cube into a filtered 2D multichannel spectrogram that enhances the SNR, and (2) utilization of convolution filters in the CNN architecture, which allows not only capturing spectral and temporal changes within each sensor but also the hierarchical analysis of the entire sensor array, including reactivity and response time relation of the sensor array. As a result, our CNN model successfully classified multiple VOC gas components with 93.9% accuracy. Our approach shows significant potential for practical applications, as it enables the detection and analysis of acetone, ethanol, and xylene, which are common yet harmful gases in the environment, with potential implications for early detection of diseases like lung cancer. The ability to accurately identify and classify these gas mixtures highlights the practical significance of this method in medical diagnostics and environmental monitoring.

MATERIALS AND METHODS

All experimental and simulation methods are described in the Supporting Information.

ASSOCIATED CONTENT

Supporting Information

The Supporting Information is available free of charge at https://pubs.acs.org/doi/10.1021/acssensors.5c00015.

https://doi.org/10.1021/acssensors.5c00015
ACS Sens. 2025, 10, 3003−3012

Detailed materials and methods description of the functionalized M13 bacteriophages, DFT molecular simulations, the experiment setup, and the deep learning CNN model; CNN classification results; gas mixture identification research summary; colorimetric sensor response measurements; hyperspectral data processing sequence; optimized geometries of amino acid-target molecules; spectral changes and color distance analysis; PCA for VOC classification; multichannel spectrograms; and ROC curve comparison for CNN-based classification (PDF)

AUTHOR INFORMATION

Corresponding Authors

Jin-Woo Oh − *BK21 FOUR Education and Research Division for Energy Convergence Technology, Bio-IT Fusion Technology Research Institute, and Department of Nano Fusion Technology Institute, Pusan National University, Busan 46241, Republic of Korea;* orcid.org/0000-0002-0065-5088; Email: ojw@pusan.ac.kr

Seungchul Kim − *Department of Cogno-Mechatronics Engineering, Pusan National University, Busan 46241, Republic of Korea; Department of Optics and Mechatronics Engineering, Pusan National University, Busan 46241, Republic of Korea;* orcid.org/0000-0002-6765-2471; Email: s.kim@pusan.ac.kr

Authors

Eunji Choi − *Department of Cogno-Mechatronics Engineering, Pusan National University, Busan 46241, Republic of Korea;* orcid.org/0009-0004-4253-1341

Tae-In Jeong − *Department of Cogno-Mechatronics Engineering, Pusan National University, Busan 46241, Republic of Korea;* orcid.org/0000-0002-7278-9237

Thanh Mien Nguyen − *BK21 FOUR Education and Research Division for Energy Convergence Technology and Bio-IT Fusion Technology Research Institute, Pusan National University, Busan 46241, Republic of Korea;* orcid.org/0000-0002-8137-4455

Alexander Gliserin − *Department of Cogno-Mechatronics Engineering, Pusan National University, Busan 46241, Republic of Korea; Department of Optics and Mechatronics Engineering, Pusan National University, Busan 46241, Republic of Korea*

Jimin Lee − *Department of Cogno-Mechatronics Engineering, Pusan National University, Busan 46241, Republic of Korea*

Gyeong-Ha Bak − *BK21 FOUR Education and Research Division for Energy Convergence Technology and Bio-IT Fusion Technology Research Institute, Pusan National University, Busan 46241, Republic of Korea*

San Kim − *Department of Cogno-Mechatronics Engineering, Pusan National University, Busan 46241, Republic of Korea*

Sehyeon Kim − *Department of Cogno-Mechatronics Engineering, Pusan National University, Busan 46241, Republic of Korea*

Complete contact information is available at: https://pubs.acs.org/10.1021/acssensors.5c00015

Author Contributions

#E.C., T.-I.J., and T.M.N. contributed equally to this work.

Notes

The authors declare no competing financial interest.

ACKNOWLEDGMENTS

This research was supported by the National Research Foundation of Korea (NRF) grant funded by the Korean government (RS-2024-00336583, RS-2024-00406152, RS-2023-00236798).

REFERENCES

(1) Li, Z.; Li, H.; LaGasse, M. K.; Suslick, K. S. Rapid quantification of trimethylamine. *Anal. Chem.* **2016**, *88* (11), 5615−5620.

(2) Lim, S. H.; Feng, L.; Kemling, J. W.; Musto, C. J.; Suslick, K. S. An optoelectronic nose for the detection of toxic gases. *Nat. Chem.* **2009**, *1* (7), 562−567.

(3) Qin, M.; Sun, M.; Bai, R.; Mao, Y.; Qian, X.; Sikka, D.; Zhao, Y.; Qi, H. J.; Suo, Z.; He, X. Bioinspired hydrogel interferometer for adaptive coloration and chemical sensing. *Adv. Mater.* **2018**, *30* (21), No. 1800468.

(4) Song, C.; Yang, B.; Zhu, Y.; Yang, Y.; Wang, L. Ultrasensitive sliver nanorods array SERS sensor for mercury ions. *Biosens. Bioelectron.* **2017**, *87*, 59−65.

(5) Peng, G.; Tisch, U.; Adams, O.; Hakim, M.; Shehada, N.; Broza, Y. Y.; Billan, S.; Abdah-Bortnyak, R.; Kuten, A.; Haick, H. Diagnosing lung cancer in exhaled breath using gold nanoparticles. *Nat. Nanotechnol.* **2009**, *4* (10), 669−673.

(6) Yu, H.; Xu, L.; Cao, M.; Chen, X.; Wang, P.; Jiao, J.; Wang, Y. In *Detection Volatile Organic Compounds in Breath as Markers of Lung Cancer Using a Novel Electronic Nose*, Proceedings of IEEE Sensors 2003 (IEEE Cat. No.03CH37498); IEEE, 2003; pp 1333−1337.

(7) Lee, J.-M.; Choi, E. J.; Chung, J. H.; Lee, K.-w.; Lee, Y.; Kim, Y.-J.; Kim, W.-G.; Yoon, S. H.; Seol, H. Y.; Devaraj, V. A DNA-derived phage nose using machine learning and artificial neural processing for diagnosing lung cancer. *Biosens. Bioelectron.* **2021**, *194*, No. 113567, DOI: 10.1016/j.bios.2021.113567.

(8) D'Amico, A.; Pennazza, G.; Santonico, M.; Martinelli, E.; Roscioni, C.; Galluccio, G.; Paolesse, R.; Di Natale, C. An investigation on electronic nose diagnosis of lung cancer. *Lung Cancer* **2010**, *68* (2), 170−176.

(9) Deshmukh, S.; Bandyopadhyay, R.; Bhattacharyya, N.; Pandey, R.; Jana, A. Application of electronic nose for industrial odors and gaseous emissions measurement and monitoring−an overview. *Talanta* **2015**, *144*, 329−340.

(10) Wang, T.; Zhang, H.; Wu, Y.; Chen, X.; Chen, X.; Zeng, M.; Yang, J.; Su, Y.; Hu, N.; Yang, Z. Classification and concentration prediction of VOCs with high accuracy based on an electronic nose using an ELM-ELM integrated algorithm. *IEEE Sens. J.* **2022**, *22* (14), 14458−14469.

(11) Peris, M.; Escuder-Gilabert, L. Electronic noses and tongues to assess food authenticity and adulteration. *Trends Food Sci. Technol.* **2016**, *58*, 40−54.

(12) Schroeder, V.; Evans, E. D.; Wu, Y.-C. M.; Voll, C.-C. A.; McDonald, B. R.; Savagatrup, S.; Swager, T. M. Chemiresistive sensor array and machine learning classification of food. *ACS Sens.* **2019**, *4* (8), 2101−2108.

(13) Qin, P.; Day, B. A.; Okur, S.; Li, C.; Chandresh, A.; Wilmer, C. E.; Heinke, L. VOC mixture sensing with a MOF film sensor array: detection and discrimination of xylene isomers and their ternary blends. *ACS Sens.* **2022**, *7* (6), 1666−1675.

(14) Chen, L.; Chen, B.; Matsuo, T.; Sassa, F.; Hayashi, K.; Chen, L. Recognition of Mixture Vapors using SERS Gas Sensor Fabricated by the Sputtering Method. *IEEE Sens. J.* **2024**, *24*, 15773−15783, DOI: 10.1109/JSEN.2024.3383053.

(15) Thai, N. X.; Tonezzer, M.; Masera, L.; Nguyen, H.; Van Duy, N.; Hoa, N. D. Multi gas sensors using one nanomaterial, temperature gradient, and machine learning algorithms for discrimination of gases and their concentration. *Anal. Chim. Acta* **2020**, *1124*, 85−93.

(16) Tonezzer, M. Selective gas sensor based on one single SnO2 nanowire. *Sens. Actuators, B* **2019**, *288*, 53−59.

(17) Wang, S.; Chen, H.; Sun, B. Recent progress in food flavor analysis using gas chromatography−ion mobility spectrometry (GC−IMS). *Food Chem.* **2020**, *315*, No. 126158.
(18) Kang, H.; Cho, S. Y.; Ryu, J.; Choi, J.; Ahn, H.; Joo, H.; Jung, H. T. Multiarray nanopattern electronic nose (E-Nose) by high-resolution top-down nanolithography. *Adv. Funct. Mater.* **2020**, *30* (27), No. 2002486.
(19) Hossein-Babaei, F.; Amini, A. A breakthrough in gas diagnosis with a temperature-modulated generic metal oxide gas sensor. *Sens. Actuators, B* **2012**, *166-167*, 419−425.
(20) Yu, C.; Han, R.; Song, M.; Liu, C.; Chang, C.-I. A simplified 2D-3D CNN architecture for hyperspectral image classification based on spatial−spectral fusion. *IEEE J. Sel. Top. Appl. Earth Obs. Remote Sens.* **2020**, *13*, 2485−2501.
(21) Ahmad, M.; Mazzara, M.; Distefano, S. Regularized CNN feature hierarchy for hyperspectral image classification. *Remote Sens.* **2021**, *13* (12), No. 2275.
(22) Cheng, G.; Li, Z.; Han, J.; Yao, X.; Guo, L. Exploring hierarchical convolutional features for hyperspectral image classification. *IEEE Trans. Geosci. Remote Sens.* **2018**, *56* (11), 6712−6722.
(23) Kim, H.-J.; Lee, J.-H. Highly sensitive and selective gas sensors using p-type oxide semiconductors: Overview. *Sens. Actuators, B* **2014**, *192*, 607−627.
(24) Zhang, B.; Cheng, M.; Liu, G.; Gao, Y.; Zhao, L.; Li, S.; Wang, Y.; Liu, F.; Liang, X.; Zhang, T.; Lu, G. Room temperature NO2 gas sensor based on porous Co3O4 slices/reduced graphene oxide hybrid. *Sens. Actuators, B* **2018**, *263*, 387−399.
(25) Acharyya, S.; Nag, S.; Kimbahune, S.; Ghose, A.; Pal, A.; Guha, P. K. Selective discrimination of VOCs applying gas sensing kinetic analysis over a metal oxide-based chemiresistive gas sensor. *ACS Sens.* **2021**, *6* (6), 2218−2224.
(26) Ingle, N.; Sayyad, P.; Deshmukh, M.; Bodkhe, G.; Mahadik, M.; Al-Gahouari, T.; Shirsat, S.; Shirsat, M. D. A chemiresistive gas sensor for sensitive detection of SO 2 employing Ni-MOF modified−OH-SWNTs and−OH-MWNTs. *Appl. Phys. A* **2021**, *127*, No. 157.
(27) van den Broek, J.; Abegg, S.; Pratsinis, S. E.; Güntner, A. T. Highly selective detection of methanol over ethanol by a handheld gas sensor. *Nat. Commun.* **2019**, *10* (1), No. 4220.
(28) Chen, W. Y.; Jiang, X.; Lai, S.-N.; Peroulis, D.; Stanciu, L. Nanohybrids of a MXene and transition metal dichalcogenide for selective detection of volatile organic compounds. *Nat. Commun.* **2020**, *11* (1), No. 1302.
(29) Li, L.; Dong, S.; Cao, S.; Chen, Y.; Shen, J.; Li, M.; Cui, Q.; Zhang, Y.; Huang, C.; Dai, Q. E-nose and colorimetric sensor array combining homologous data fusion strategy discriminating the roasting degree of large-leaf yellow tea. *Food Chem.:X* **2024**, *21*, No. 101124.
(30) VS, A. P.; Joseph, P.; SCG, K. D.; Lakshmanan, S.; Kinoshita, T.; Muthusamy, S. Colorimetric sensors for rapid detection of various analytes. *Mater. Sci. Eng.: C* **2017**, *78*, 1231−1245.
(31) Wilson, A. D.; Baietto, M. Applications and advances in electronic-nose technologies. *Sensors* **2009**, *9* (7), 5099−5148.
(32) Shang, L.; Zhang, W.; Xu, K.; Zhao, Y. Bio-inspired intelligent structural color materials. *Mater. Horiz.* **2019**, *6* (5), 945−958.
(33) Askim, J. R.; Li, Z.; LaGasse, M. K.; Rankin, J. M.; Suslick, K. S. An optoelectronic nose for identification of explosives. *Chem. Sci.* **2016**, *7* (1), 199−206.
(34) Im, H.; Choi, J.; Lee, H.; Al Balushi, Z. Y.; Park, D. H.; Kim, S. Colorimetric Multigas Sensor Arrays and an Artificial Olfactory Platform for Volatile Organic Compounds. *ACS Sens.* **2023**, *8* (9), 3370−3379.
(35) Engel, L.; Benito-Altamirano, I.; Tarantik, K. R.; Pannek, C.; Dold, M.; Prades, J. D.; Wöllenstein, J. Printed sensor labels for colorimetric detection of ammonia, formaldehyde and hydrogen sulfide from the ambient air. *Sens. Actuators, B* **2021**, *330*, No. 129281.
(36) Jeong, T.-I.; Nguyen, T. M.; Choi, E.; Gliserin, A.; Nguyen, T. M.; Kim, S.; Kim, S.; Kim, H.; Bak, G.-H.; Kim, N.-Y.; et al. Multichannel Hierarchical Analysis of Time-Resolved Hyperspectral Data for Advanced Colorimetric E-Nose. *ACS Sens.* **2024**, *9* (6), 2869−2876.
(37) Oguma, T.; Nagaoka, T.; Kurahashi, M.; Kobayashi, N.; Yamamori, S.; Tsuji, C.; Takiguchi, H.; Niimi, K.; Tomomatsu, H.; Tomomatsu, K.; et al. Clinical contributions of exhaled volatile organic compounds in the diagnosis of lung cancer. *PLoS One* **2017**, *12* (4), No. e0174802.
(38) Dick, R. B.; Brown, W. D.; Setzer, J. V.; Taylor, B. J.; Shukia, R. Effects of short duration exposures to acetone and methyl ethyl ketone. *Toxicol. Lett.* **1988**, *43* (1−3), 31−49.
(39) Nguyen, T. M.; Jang, W. B.; Lee, Y.; Kim, Y. H.; Lim, H. J.; Lee, E. J.; Nguyen, T. M.; Choi, E.-J.; Kwon, S.-M.; Oh, J.-W. Non-intrusive quality appraisal of Differentiation-induced cardiovascular stem cells using E-Nose sensor technology. *Biosens. Bioelectron.* **2024**, *246*, No. 115838.
(40) Chung, W.-J.; Oh, J.-W.; Kwak, K.; Lee, B. Y.; Meyer, J.; Wang, E.; Hexemer, A.; Lee, S.-W. Biomimetic self-templating supramolecular structures. *Nature* **2011**, *478* (7369), 364−368.
(41) Oh, J.-W.; Chung, W.-J.; Heo, K.; Jin, H.-E.; Lee, B. Y.; Wang, E.; Zueger, C.; Wong, W.; Meyer, J.; Kim, C.; et al. Biomimetic virus-based colourimetric sensors. *Nat. Commun.* **2014**, *5* (1), No. 3043.
(42) Feng, F.; Li, W.; Du, Q.; Zhang, B. Dimensionality reduction of hyperspectral image with graph-based discriminant analysis considering spectral similarity. *Remote Sens.* **2017**, *9* (4), No. 323.
(43) Signoroni, A.; Savardi, M.; Baronio, A.; Benini, S. Deep learning meets hyperspectral image analysis: A multidisciplinary review. *J. Imaging* **2019**, *5* (5), No. 52.
(44) Hidalgo, D. R.; Cortés, B. B.; Bravo, E. C. Dimensionality reduction of hyperspectral images of vegetation and crops based on self-organized maps. *Inf. Process. Agric.* **2021**, *8* (2), 310−327.
(45) Lee, J.-M.; Lee, Y.; Devaraj, V.; Nguyen, T. M.; Kim, Y.-J.; Kim, Y. H.; Kim, C.; Choi, E. J.; Han, D.-W.; Oh, J.-W. Investigation of colorimetric biosensor array based on programable surface chemistry of M13 bacteriophage towards artificial nose for volatile organic compound detection: From basic properties of the biosensor to practical application. *Biosens. Bioelectron.* **2021**, *188*, No. 113339.
(46) Jeon, D.; Kim, M.-S. Deep-Learning-Based Sequence Causal Long-Term Recurrent Convolutional Network for Data Fusion Using Video Data. *Electronics* **2023**, *12* (5), No. 1115.
(47) Paoletti, M. E.; Haut, J. M.; Plaza, J.; Plaza, A. Deep learning classifiers for hyperspectral imaging: A review. *ISPRS J. Photogramm. Remote Sens.* **2019**, *158*, 279−317.
(48) Valizadeh, M.; Wolff, S. J. Convolutional Neural Network applications in additive manufacturing: A review. *Adv. Ind. Manuf. Eng.* **2022**, *4*, No. 100072.
(49) Cho, I.; Lee, K.; Sim, Y. C.; Jeong, J.-S.; Cho, M.; Jung, H.; Kang, M.; Cho, Y.-H.; Ha, S. C.; Yoon, K.-J.; Park, I. Deep-learning-based gas identification by time-variant illumination of a single micro-LED-embedded gas sensor. *Light: Sci. Appl.* **2023**, *12* (1), No. 95.
(50) Hwang, Y. J.; Yu, H.; Lee, G.; Shackery, I.; Seong, J.; Jung, Y.; Sung, S.-H.; Choi, J.; Jun, S. C. Multiplexed DNA-functionalized graphene sensor with artificial intelligence-based discrimination performance for analyzing chemical vapor compositions. *Microsyst. Nanoeng.* **2023**, *9* (1), No. 28.
(51) Chu, J.; Li, W.; Yang, X.; Wu, Y.; Wang, D.; Yang, A.; Yuan, H.; Wang, X.; Li, Y.; Rong, M. Identification of gas mixtures via sensor array combining with neural networks. *Sens. Actuators, B* **2021**, *329*, No. 129090.
(52) Lv, S.; Gu, T.; Wang, J.; Pan, S.; Liu, F.; Sun, P.; Wang, L.; Lu, G. Pattern recognition with temperature regulation: A single YSZ-based mixed potential sensor classifies multiple mixtures of isoprene, n-propanol, and acetone. *ACS Sens.* **2023**, *8* (11), 4323−4333.

https://doi.org/10.1021/acssensors.5c00015
ACS Sens. 2025, 10, 3003−3012